

Investigation of the Exclusive ${}^3\text{He}(e,e'pn)p$ Reaction

D.G. Middleton,^{1,*} J.R.M. Annand,² M. Ases Antelo,³ C. Ayerbe,³ P. Barneo,⁴ D. Baumann,³ J. Bermuth,³ J. Bernauer,³ H.P. Blok,^{4,5} D. Bosnar,⁶ R. Böhm,³ M. Ding,³ M.O. Distler,³ J. Friedrich,³ J. García Llongo,³ D.I. Glazier,² J. Golak,⁷ W. Glöckle,⁸ P. Grabmayr,¹ T. Hehl,¹ J. Heim,¹ W.H.A. Hesselink,^{4,5} E. Jans,⁴ H. Kamada,⁹ G. Jover Mañas,³ M. Kohl,³ L. Lapikás,⁴ I.J.D. MacGregor,² I. Martin,¹ J.C. McGeorge,² H. Merkel,³ P. Merle,³ K. Monstad,² F. Moschini,¹ U. Müller,³ A. Nogga,¹⁰ R. Pérez Benito,³ Th. Pospischil,³ M. Potokar,¹¹ G. Rosner,² M. Seimetz,³ R. Skibiński,⁷ H. de Vries,⁴ Th. Walcher,³ D.P. Watts,² M. Weinriefer,³ M. Weiss,³ H. Witała,⁷ and B. Zihlmann^{4,5}

¹Kepler Centre for Astro and Particle Physics, Physikalisches Institut, Universität Tübingen, D-72076 Tübingen, Germany

²Department of Physics and Astronomy, University of Glasgow, Glasgow G12 8QQ, Scotland

³Institut für Kernphysik, Johannes Gutenberg-Universität Mainz, D-55099 Mainz, Germany

⁴Nikhef, P.O. Box 41882, 1009 DB Amsterdam, The Netherlands

⁵Dept. of Physics, VU-university, Amsterdam, The Netherlands

⁶Department of Physics, University of Zagreb, Croatia

⁷M. Smoluchowski Institute of Physics, Jagiellonian University, PL-30059 Kraków, Poland

⁸Institut für Theoretische Physik II, Ruhr-Universität Bochum, D-44780 Bochum, Germany

⁹Department of Physics, Faculty of Engineering,

Kyushu Institute of Technology, Kitakyushu 804-8550, Japan

¹⁰Institute for Advance Simulation, Institut für Kernphysik,

and Jülich Center for Hadron Physics, Forschungszentrum Jülich, D-52425 Jülich, Germany

¹¹Institute Jožef Stefan, University of Ljubljana, Ljubljana, Slovenia

(Dated: 3rd November 2018)

Cross sections for the ${}^3\text{He}(e,e'pn)p$ reaction were measured for the first time at energy transfers of 220 and 270 MeV for several momentum transfers ranging from 300 to 450 MeV/ c . Cross sections are presented as a function of the momentum of the recoil proton and the momentum transfer. Continuum Faddeev calculations using the Argonne V18 and Bonn-B nucleon-nucleon potentials overestimate the measured cross sections by a factor 5 at low recoil proton momentum with the discrepancy becoming much smaller at higher recoil momentum.

PACS numbers: 25.10.+s, 25.30.Fj, 21.45.-v, 21.30.Fe, 13.75.Cs

The understanding of nucleon-nucleon (NN) interactions within the nucleus is of great importance for modern nuclear physics. These NN interactions, which are characterised at short inter-nucleon separations by a strong scalar repulsive component and at intermediate to large separations by an attractive part, caused mainly by the strong tensor component of the meson-exchange contribution, induce correlations between the nucleons. The use of electron-induced exclusive two-nucleon knockout reactions of the type $A(e,e'pN)A-2$ is a very direct method for the study of this correlated behaviour within the nucleus. Because the scalar and tensor interactions act differently in isospin $T = 0$ and $T = 1$ states proton-proton and proton-neutron knockout reactions probe predominantly the short-range and tensor component, respectively [1, 2].

The use of ${}^3\text{He}$ as a laboratory for the study of NN correlations via $(e,e'pN)N$ reactions has advantages, both experimentally and theoretically, over other nuclei. From an experimental point of view the final state is a single nucleon in its ground state so detector resolution is not

critical and reconstruction of the final state is straightforward. Furthermore theoretical models exist [3, 4, 5] that allow the break-up cross section to be calculated exactly, with interactions between all three nucleons being completely taken into account. Such models calculate both the ${}^3\text{He}$ ground state and the three-nucleon continuum wave functions using realistic NN potentials which include a phenomenological description of the short range part of the NN interaction [6, 7].

At electron energies of several hundred MeV the electron-induced two-nucleon knockout cross section is driven by several processes. The coupling of the virtual photon to one nucleon of a correlated pair via one-body hadronic currents can lead to the ejection of both nucleons from the nucleus. Interaction of the virtual photon with two-body hadronic currents, such as meson exchange currents (MEC) or isobar currents (IC), also contributes to the cross section. In addition to the above processes there can also be interactions between all particles in the final state (FSI), the strength of which depends strongly on the relative nucleon-nucleon energies. The relative importance of these different processes depends on the kinematics and type of reaction. In order to disentangle these different contributing processes it is important to measure both the $(e,e'pp)$ and $(e,e'pn)$

*Electronic address: duncan@pit.physik.uni-tuebingen.de

cross sections as a function of several kinematic variables. The ${}^3\text{He}(e, e'pp)n$ reaction was studied previously in [8, 9, 10]. Here we present the results of a measurement of the ${}^3\text{He}(e, e'pn)p$ reaction made in the so-called “dip-region” between quasi-elastic and Δ -excitation peaks in the inclusive electron-scattering spectrum.

The measurements were performed at the electron scattering facility of the 100% duty factor Mainz Microtron MAMI [11, 12]. The 855 MeV electron beam, used with currents between 2 and 4 μA , was incident on a ${}^3\text{He}$ high-pressure cryogenic gas target, operated at 1.9 MPa and 15 K. At 4 μA beam current this corresponds to a luminosity of $2 \times 10^{36} \text{ cm}^{-2} \text{ s}^{-1}$. The scattered electrons were detected in Spectrometer B [13], a magnetic spectrometer with a solid angle of $\Delta\Omega = 5.6 \text{ msr}$ and momentum acceptance of $\Delta p/p = 15\%$. The ejected protons were detected using the scintillator detector HADRON3 (H3) [14] from Nikhef, a large solid angle ($\Delta\Omega = 230 \text{ msr}$) hodoscope consisting of 128 bars of plastic scintillator divided into eight layers: two hodoscope layers at the front with six energy-determining layers behind. The proton energy acceptance of H3 is 50 - 250 MeV. For detection of the ejected neutrons the Glasgow-Tübingen time-of-flight (TOF) detector system [15] was used. The TOF detector array consisted of 96 bars of plastic scintillator arranged in three stands of 32 bars. Each stand consisted of 4 layers of 8 detectors, 3 layers of 5 cm thick TOF bars positioned behind a layer of 8 overlapping 1 cm thick veto detectors in a configuration similar to that described in [16]. The TOF array covered a solid angle of $\Delta\Omega \approx 240 \text{ msr}$.

Kinematics were chosen so that the reaction could be studied over a range of energy and momentum transfers similar to that covered previously in a measurement of the ${}^3\text{He}(e, e'pp)n$ reaction [9]. The settings used for each of the different kinematics studied are summarised in table I. Data were taken at momentum transfers of $q = 300$ and $375 \text{ MeV}/c$ for an energy transfer of $\omega = 220 \text{ MeV}$ and at momentum transfers of $q = 330, 375$ and $450 \text{ MeV}/c$ for an energy transfer of $\omega = 270 \text{ MeV}$. The proton detector, H3, was positioned in the direction of the momentum transfer \vec{q} at forward angles with respect to the beam on the opposite side of the beam line to Spectrometer B while the TOF neutron detectors were positioned at 180° to the direction of \vec{q} at backward angles with respect to the beam on the same side as Spectrometer B. After software cuts the neutron energy threshold in TOF was 16.7 MeV, while the use of 0.5 cm thick lead shielding in front of H3 resulted in an effective proton energy threshold of 70 MeV.

With the detection of two ejected nucleons from the initial 3N -system, the kinematics of the reaction are completely determined. The missing momentum of the reaction is defined as

$$\vec{p}_m = \vec{q} - \vec{p}_{p'} - \vec{p}_{n'} \quad (1)$$

and is equal to the momentum of the undetected proton,

\vec{p}_r ; here $\vec{p}_{p'}$ and $\vec{p}_{n'}$ are the momenta of the detected proton and neutron, respectively. Using \vec{p}_m , the missing-energy

$$E_m = \omega - T_{p'} - T_{n'} - T_{r'} \quad (2)$$

can be determined where $T_{p'}$, $T_{n'}$ and $T_{r'}$ are the kinetic energies of the proton, neutron and undetected proton, respectively.

The missing-energy spectrum for the Z2 kinematic setting is shown in Fig. 1. The inset of Fig. 1 shows the missing-energy spectrum before the subtraction of accidental coincidences as well as the spectra for the different types of accidental coincidences. The $(e'p)$ and $(e'n)+(pn)$ types of accidental coincidences (red dashed and blue dotted curves) were subtracted from the total coincidence yield (black curve). As this subtracts the “ e', p, n accidental” coincidences twice (green dot-dashed curve) these were added to the result to obtain the number of real coincident events. More details of the accidental subtraction procedure can be found in reference [16]. The largest contribution to the background is from events consisting of a real coincident $(e'p)$ pair and an accidental neutron. The missing-energy spectrum corrected for accidental coincidences has a single peak which corresponds to the three-body break-up of ${}^3\text{He}$. The peak has a FWHM of 7.0 MeV, as expected from the known detector resolutions in energy and angle, and a mean value of 6.2 MeV, close to the expected value of 7.72 MeV. The tail at higher missing energies is due to radiative processes.

The 8-fold differential cross section for the ${}^3\text{He}(e, e'pn)$ reaction can be written as a 5-fold differential cross section, $d^5\sigma/dS d\Omega_p d\Omega_n$, containing the nuclear structure information, multiplied by a virtual-photon flux factor Γ_v [17]. The cross section is differential in S , where dS is the arc-length in the $T_{p'} - T_{n'}$ plane along the curve S that describes the relation between $T_{p'}$ and $T_{n'}$ for a given proton-neutron angular configuration as given by Eq. 2 [18, 19]. It depends on seven independent kinematic variables, but because of the limited statistics of the data, it will be presented as function of one of them only, integrating over the others within the acceptance of the detectors. The average 5-fold experimental cross section was calculated as:

$$\frac{d^5\sigma}{dS d\Omega_p d\Omega_n}(x) = \frac{1}{\int \mathcal{L} dt} \frac{N(x, \Delta x)}{\mathcal{V}(x, \Delta x)} \quad (3)$$

where Δx represents a range (bin) in the variable x as a function of which the cross section is presented, $\int \mathcal{L} dt$ is the integrated luminosity, $N(x, \Delta x)$ is the measured number of $(e, e'pn)$ events in bin Δx , corrected for accidental coincidences, integrated over the missing-energy range from below the peak up to 36 MeV, and $\mathcal{V}(x, \Delta x)$ is the corresponding (weighted) detection volume. The latter was determined by a Monte Carlo method using 10^8 events, generated within the energy/momentum ac-

Label	ω [MeV]	q [MeV/c]	θ_B [deg]	θ_{H3} [deg]	θ_{TOF-1} [deg]	θ_{TOF-2} [deg]	θ_{TOF-3} [deg]	θ_q [deg]
A1	220	375	23.8	-53.3	107.7	125.5	140.5	-43.1
A2	270	375	20.9	-44.0	107.7	125.5	140.5	-34.3
B2	270	450	29.3	-44.0	107.7	125.5	140.5	-39.8
Y1	220	300	15.4	-45.0	107.7	125.5	140.5	-35.5
Z2	270	330	15.9	-45.0	107.7	125.5	140.5	-28.1

Table I: Kinematic settings in which the data were taken. The detector angles given are the central angle of each detector in the lab frame.

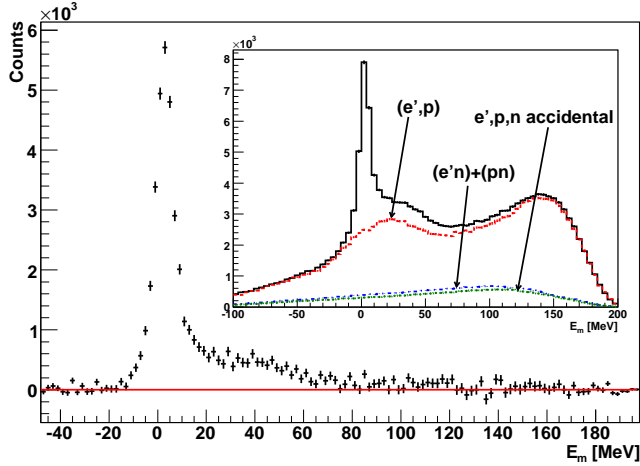


Figure 1: (colour online). The missing-energy (E_m) distribution for the ${}^3\text{He}(e, e'pn)$ reaction for the Z2 kinematic setting. The inset shows the E_m distribution before subtraction of accidental coincidences. The black curve results from all $(e'pn)$ events in a coincidence time region where real triple-coincidence events would be found. The dashed red curve shows the contribution from events with an accidental neutron, the dot-dashed blue curve shows the contribution from events with an accidental proton or electron and the dotted green line shows the contribution from events where all three particles are in accidental coincidence.

ceptances of the three detectors involved, taking into account energy conservation for the reaction. This yielded an eight-dimensional phase-space or detection volume \mathcal{V} . Radiative corrections were applied to the phase space which were calculated using the formalism of Mo and Tsai [20]. The factor Γ_v was also included as a weight, as were the efficiencies of the H3 and TOF detectors. The former ranged from 90% to 80% depending on the proton energy. The neutron detection efficiency was about 2.7% on average for a 5 cm thick TOF bar at the signal pulse-height threshold used. This energy dependent efficiency was computed with a model based on the Stanton code [21, 22]. Finally the phase space was integrated over the missing-energy to yield $\mathcal{V}(x, \Delta x)$ using the same limits as in the determination of $N(x, \Delta x)$, and over all variables except x , applying the same cuts in $T_{p'}$ and $T_{n'}$ as for the experimental data. The statistical error associated

with the generated phase-space is $\leq 0.5\%$. Corrections for dead time in the electronics were included in the determination of the integrated luminosity $\int \mathcal{L} dt$.

In the figures only the statistical errors are shown. The overall systematic error is about 13% with the largest contribution coming from the uncertainty ($\approx 12\%$) in the neutron detection efficiency. The uncertainty in the correction for hadronic interactions and multiple scattering in H3 is about 4%. Other contributions to the systematic error such as those from luminosity calibration, dead time corrections and target-thickness determination from elastic scattering, are negligible compared to those of the detection efficiency corrections.

The measured cross sections are compared to the results of non-relativistic continuum Faddeev calculations [4] using the Argonne V18 and Bonn-B nucleon-nucleon potentials. The calculations contain mechanisms for photon absorption on one, two or all three of the nucleons in the target but are limited in their treatment of exchange and isobar currents. The calculations are only strictly applicable for photon energies below pion production threshold. Rescattering processes up to all orders in the continuum are included ensuring that all FSI effects are fully taken into account. Two types of calculations were made. The first employed only a one-body hadronic current operator, while the second also included a two-body current operator for π and ρ mesons to account for the in-flight and seagull terms using the formalism of Schiavilla *et al.* [23] which is based on earlier work of Riska [24, 25].

For comparison to the measured data the calculation of the theoretical cross sections was done in two steps. In the first part the Faddeev equations were solved for a single, central (ω, q) point per kinematic setting. All NN -force components were included up to a two-body angular momentum of $j = 3$ and in the final state all partial waves were included up to three-body angular momentum $J = \frac{15}{2}$. Then, in the second step, the cross section was calculated for many specific three-nucleon final states determined by $\vec{p}_{p'}$ and $\vec{p}_{n'}$ for a given (ω, q) point. The final states were randomly generated over the full acceptance of the H3 and TOF detectors using a generator similar to that used for the phase space. Approximately 10^7 events were generated for each (ω, q) point to ensure full coverage and to reduce statistical fluctuations. Then the average cross section as a function of

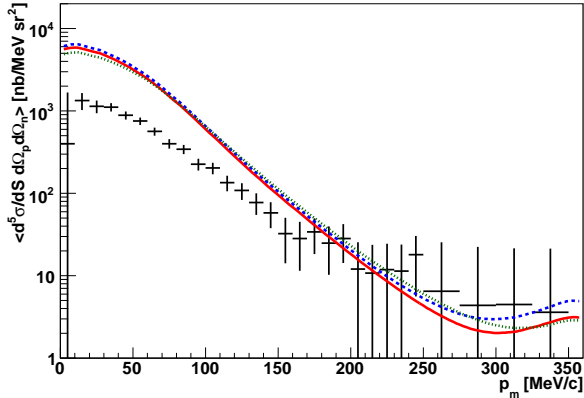


Figure 2: (colour online). The cross section for the ${}^3\text{He}(e,e'pn)$ reaction shown as a function of the missing momentum for the A1 kinematic setting. The solid red (dotted green) curve shows the theoretical cross section calculated using only a one-body hadronic current operator and the Argonne V18 (Bonn-B) NN potential. The dashed blue line results from the Argonne potential when MECs are also included.

one variable integrated over all the others was calculated. This method of determining the theoretical cross section for a given experimental set-up is more accurate than that used previously for comparison to the measurement of the ${}^3\text{He}(e,e'pp)$ reaction [9] where the cross sections were calculated for a grid of points covering the energy and angular acceptances of the two proton detectors.

The effect of using only the central (ω, q) point was investigated for one kinematic setting. The average difference in the calculated theoretical cross section between using just the central value or using a range covering the whole acceptance of spectrometer B was found to be about 10%.

Fig. 2 shows the ${}^3\text{He}(e,e'pn)$ cross section as a function of the missing momentum for the A1 kinematic setting. The solid red line shows the theoretical cross section calculated using the Argonne V18 NN potential and a one-body hadronic current operator, while the dashed blue line shows the results when MECs are also included. The dotted green line in Fig. 2 shows the result of the one-body calculation using the Bonn-B NN potential.

In Fig. 2 the overall shape of the measured and theoretical cross sections is similar in that they decrease roughly exponentially with increasing p_m . The inclusion of the MECs increases the calculated cross section by only about 10% up to $p_m = 200$ MeV/c but the effect increases to about 60% at 350 MeV/c. The use of the two different potentials makes little difference to the results of the calculations which overpredict the experimental data by about a factor of 5 for $p_m \leq 80$ MeV/c. The discrepancy decreases with increasing p_m until rough agreement within the large experimental error bars is reached at $p_m \approx 200$ MeV/c. In general the calculations indicate that

for the kinematics shown here the ${}^3\text{He}(e,e'pn)$ cross section is dominated by the one-body hadronic current term with MECs only making a minor contribution.

The overprediction of the cross section by the theoretical calculations is in contrast to the ${}^3\text{He}(e,e'pp)$ reaction [9] where calculations using the Bonn-B potential are slightly below the data at low p_m and a factor of 5 lower at $p_m = 200$ MeV/c. There is not only a clear difference in the ratio between the pp and pn -knockout data and their respective one-body current prediction, but also the measured cross sections do not fall as quickly as predicted with increasing p_m .

This different behaviour between pp and pn knockout is intriguing. The large discrepancy at low p_m in the case of pn knockout, where the virtual photon supposedly couples mainly to one of the nucleons of a pn pair, would suggest that the pn correlations in the probed regime are not well predicted by the theory. Another source of disagreement could be the incomplete treatment of MECs and the omission of ICs, which play a much larger role in pn than in pp knockout. Finally, as stated above, the theory is only applicable for photon energies below pion production threshold.

Fig. 3 shows the ${}^3\text{He}(e,e'pn)$ cross section as a function of q for the ω range $235 \leq \omega \leq 265$ MeV and the p_m range $50 \leq p_m \leq 100$ MeV/c. The experimental cross section in Fig. 3 was measured in five different kinematic settings, shown by the different types of markers for the data points, and shows a smoothly rising q -dependence which increases by about a factor 2 in strength from $q = 300$ to 450 MeV/c. The line convention for the theoretical curves is the same as for Fig. 2. The theoretical cross sections were calculated for five separate q -values which are indicated by the filled black circles in the curves. The theoretical calculations over-predict the measured cross sections for the whole q range covered; by a factor 2-3 at $q = 320$ MeV/c to a factor of about 5 at $q = 450$ MeV/c. The inclusion of the MECs increases the calculated cross section by about 30% at $q = 320$ MeV/c. This increase falls with increasing q to about 5% at $q = 450$ MeV/c.

The q -dependence of the ${}^3\text{He}(e,e'pp)$ data for a similar p_m range is much better described by the calculations with just a q -independent under-prediction of 20%. Again this points to an inadequacy in the theoretical calculations for pn knockout, as discussed above.

In conclusion the ${}^3\text{He}(e,e'pn)$ reaction was measured with good statistical accuracy over a range of momentum transfers and for two energy transfers. Calculations using the Argonne V18 or Bonn B potentials over-predict the measured cross sections by a factor 5 at low p_m but are in rough agreement within the large statistical experimental errors at $p_m \geq 200$ MeV/c. Inclusion of MECs increases the calculated cross section by a small amount (about 10%) up to $p_m = 200$ MeV/c, increasing to about 60% at $p_m = 350$ MeV/c. When the cross section at low p_m is considered as a function of q the calculations over-predict the data by a factor 2 to 5.

Comparison with data measured for the ${}^3\text{He}(e,e'pp)$

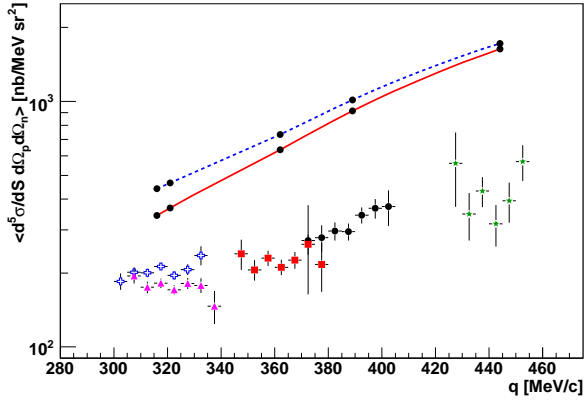


Figure 3: (colour online). The cross section for the ${}^3\text{He}(e,e'pn)$ reaction shown as a function of q for $50 \leq p_m \leq 100$ MeV/ c and $235 \leq \omega \leq 265$ MeV. Results from different kinematic settings are shown by the different types of markers for the data points: A1: black circles; A2: red squares; B2: green stars; Y1: magenta triangles; Z2: blue crosses. The same line convention is used for the theoretical curves as in Fig. 2. The theoretical cross section was calculated at the points in the curves indicated by the black circles.

reaction, which are much better described by the same theoretical calculations at low p_m , suggests that the pn correlations in the probed kinematical regime are not well described and/or reaction mechanisms that are not included in the calculations (such as isobar currents and certain meson-exchange currents) play a large role.

Acknowledgments

The authors would like to thank the staff of the Institut für Kernphysik in Mainz for providing the facilities for this experiment. This work was sponsored by the UK Engineering and Physical Sciences Research Council (EPSRC), the Deutsche Forschungsgemeinschaft (DFG) and the Foundation for Fundamental Research of Matter (FOM), which is financially supported by the Netherlands Organisation for Scientific Research (NWO). It was also partially supported by the 2008-2011 Polish Science Funds as a research project No. NN202 077435. The numerical calculations were performed at the NIC, Jülich, Germany.

- [1] R. Schiavilla, R.B. Wiringa, S.C. Pieper and J. Carlson, Phys. Rev. Lett. **98**, 132501 (2007).
- [2] R. B. Wiringa, R. Schiavilla, S.C. Pieper and J. Carlson, Phys. Rev. C **78**, 021001(R) (2008).
- [3] E. van Meijgaard and J. A. Tjon, Phys. Rev. C **45**, 1463 (1992).
- [4] J. Golak, R. Skibiński, H. Witała, W. Glöckle, A. Nogga, H. Kamada, Phys. Rept. **415**, 89 (2005).
- [5] A. Deltuva, L.P. Yuan, J. Adam and P.U. Sauer, Phys. Rev. C **70**, 034004 (2004).
- [6] J. Carlson and R. Schiavilla, Rev. Mod. Phys. **70**, 743 (1998).
- [7] A. Nogga, H. Kamada, W. Glöckle and B.R. Barrett, Phys. Rev. C **65**, 054003 (2002).
- [8] D. L. Groep *et al.*, Phys. Rev. Lett. **83**, 5443 (1999).
- [9] D. L. Groep *et al.*, Phys. Rev. C **63**, 014005 (2000).
- [10] R. A. Niyazov *et al.*, Phys. Rev. Lett. **92**, 052303 (2004).
- [11] H. Herminghaus *et al.*, Nucl. Instr. and Meth. in Phys. Res. A **138**, 1 (1976).
- [12] Th. Walcher, Prog. Part. Nucl. Phys. **24**, 189 (1990).
- [13] K. I. Blomqvist *et al.*, Nucl. Instr. and Meth. in Phys. Res. A **403**, 263 (1998).
- [14] A. Pellegrino *et al.*, Nucl. Instr. and Meth. in Phys. Res. A **437**, 188 (1999).
- [15] P. Grabmayr *et al.*, Nucl. Instr. and Meth. in Phys. Res. A **402**, 85 (1998).
- [16] D. G. Middleton *et al.*, Eur. Phys. J. A **29**, 261 (2006).
- [17] F. Halzen and A. D. Martin, *Quarks and leptons* (J. Wiley and sons, 1984).
- [18] J. Golak, H. Kamada, H. Witała, W. Glöckle and S. Ishikawa, Phys. Rev. C **51**, 1638 (1995).
- [19] G. G. Ohlsen, Nucl. Instr. and Meth. **37**, 240 (1962).
- [20] L. Mo and Y. Tsai, Rev. Mod. Phys. **41**, 205 (1969).
- [21] R. M. Edelman *et al.*, Nucl. Instr. and Meth. **100**, 355 (1972).
- [22] R. A. Cecil *et al.*, Nucl. Instr. and Meth. **161**, 439 (1979).
- [23] R. Schiavilla, V. R. Pandharipande and D.O. Riska, Phys. Rev. C **40**, 2294 (1989).
- [24] D.O. Riska, Phys. Scr. **31**, 107 (1985).
- [25] D.O. Riska, Phys. Scr. **31**, 471 (1985).